

Determination of the Hurst Exponent by use of Wavelet Transforms

Ingve Simonsen* and Alex Hansen†

Institutt for fysikk, Norges Teknisk-Naturvitenskapelige Universitet, NTNU, N-7034 Trondheim, Norway

Olav Magnar Nes‡

IKU Petroleum Research, N-7034 Trondheim, Norway

(February 1, 2008)

We propose a new method for (global) Hurst exponent determination based on wavelets. Using this method, we analyze synthetic data with predefined Hurst exponents, fracture surfaces and data from economy. The results are compared to those obtained with Fourier spectral analysis. When many samples are available, the wavelet and Fourier methods are comparable in accuracy. However, when one or only a few samples are available, the wavelet method outperforms the Fourier method by a large margin.

I. INTRODUCTION

It has been known for quite some time that self-affine surfaces are abundant in nature. They can be found in various areas of natural science such as surface growth [1,2], fractured surfaces [3], geological structures [4], biological systems [5]. Even the mercantile community has reported such structures [6] (and references therein).

Self-affine surfaces in d -dimensional space are described by a set of up to $d - 1$ roughness exponents. To know these exponents have many important physical implications. First of all, if we know all the roughness exponents, we have full control of the asymptotic statistical properties of the structure. Furthermore, for instance in fracture propagation [3], the exponents are essential in order to determine the universality class of the problem.

It is quite difficult to estimate these exponents from experimental data. Too often statements are made which are based on rather marginal data analysis. It is therefore important to search for alternative ways of analyzing the data — even if the new methods are not better than those already in existence. More tools to analyze the data, widens the possibility to cross-check the conclusions. It is in this spirit that we present in this paper a new method for determining roughness exponents. The strong point of this new method is its excellent averaging properties that makes it possible to extract roughness exponents with high precision even when one or only a few samples are available.

Traditionally, the methods used to determine the self-affine exponents are done in $(1 + 1)$ -dimensions ($d = 2$). In this case we have a single global (self-affine) exponent and it is usually referred to as the *Hurst* or roughness exponent. Over the last decade or so, several different methods have been developed in order to measure this exponent from experimental data (see Ref. [7] and references therein). The most popular method is the *Fourier power spectrum method* (FPS) and we will use this method as “reference” here. A systematic study of the quality of this and other traditional methods is found in Ref. [7]. It should be pointed out that the method described in this paper, such as the FPS-method, is only valid for self-affine structure described by a global Hurst exponent.

The wavelet transform is an integral transform developed in the early eighties in signal analysis and is today used in different fields ranging from quantum physics and cosmology to data compression technology. Since the late eighties, wavelets have been an active research field in pure and applied mathematics, and large theoretical progress has been made. The wavelet transform behaves as a mathematical microscope which decomposes an input signal into amplitudes which depend on position and scale. For this purpose localized functions, called wavelets, are being used. By changing the scale of the wavelet, one is able at a certain location to focus on details at higher and higher resolution. By taking advantage of the central properties of self-affine functions, we derive a scaling relation between wavelet amplitudes at different scales, from which the Hurst exponent can be extracted. The method is easily generalized to higher dimensions.

*Ingve.Simonsen@phys.ntnu.no

†Alex.Hansen@phys.ntnu.no

‡Olav-Magnar.Nes@iku.sintef.no

To our knowledge, two papers discuss wavelet based techniques in connection with Hurst exponent measurements [8,9]. In [8], the wavelet transform modulus maxima method is introduced, and in [9], wavelet packet analysis is used to extract the Hurst exponent. The method we present here differs from both of these. We would also like to mention two other papers which discuss self-affine fractals by using wavelets [10,11]. However, these two papers are mainly concerned about the so-called inverse fractal problem for self-affine fractals and not measuring of Hurst exponents.

This paper is organized as follows. In Sec. II we review the central properties of self-affine surfaces, while in Sec. III the wavelet transform is reviewed. Sec. IV presents the derivation of the scaling relation for self-affine functions in the wavelet domain. In Sec. V this scaling relation is applied to synthetic and experimental data, and Hurst exponents are extracted. Finally, in Sec. VI, our conclusion is presented.

II. SELF AFFINE SURFACES

As stated in the introduction, self-affine surfaces, which are generalizations of Brownian motion [12,13], have statistical properties characterized by a set of exponents. Let us assume that we have a function, $h(x)$, of one variable only (for simplicity), i.e., a fractional Brownian motion [12,13]. Here x is the horizontal variable, while h is the vertical one. Self-affinity is defined through statistical invariance under the transformation

$$x \rightarrow \lambda x, \quad (1a)$$

$$h \rightarrow \lambda^H h. \quad (1b)$$

Here H is the Hurst exponent. By combining such transformations, one can construct the affine group. Thus, self-affine surfaces are (statistically) invariant under the affine group. An alternative way of expressing this invariance is by the relation

$$h(x) \simeq \lambda^{-H} h(\lambda x). \quad (2)$$

Here the symbol \simeq means statistical equality. This form will prove useful later. The Hurst exponent, H , is limited to the range $0 \leq H \leq 1$. The lower limit comes from requiring the surface width to decrease when smaller sections of the surface is studied (the opposite being unphysical), while the upper limit comes from assuming the surface to be asymptotically flat.

Eqs. (1) and (2) express that for self-affine functions one must rescale the horizontal and vertical direction differently in order to have statistical invariance. Thus, self-affine surfaces are by construction anisotropic in the horizontal and vertical direction, except when $H = 1$ (self-similarity). The Hurst exponent, H , expresses the tendency for $dh = (dh(x)/dx)dx$ to change sign. When $H = 1/2$ (Brownian motion), the sign of dh changes randomly, and the corresponding surface possesses no spatial correlations. When $1/2 < H \leq 1$, the sign tends not to change, while for $0 \leq H < 1/2$, there is a tendency for the sign to change (anti-correlation). In both intervals there are long-range correlations falling off as a power law. Surfaces with $H > 1/2$ are said to be persistent, and those with $H < 1/2$ are anti-persistent.

III. THE WAVELET TRANSFORM

Here we review some of the important properties of wavelets, without any attempt at being complete. Rather, our aim is to provide enough background for the discussion that follows. For a more complete treatment of wavelets, see e.g. Ref. [14].

In physics and mathematics there are many examples of problems which are more easily solved in a new set of coordinates (basis), where the Fourier transform being the most famous one. Such transforms consist in calculating the amplitudes for each basis function of the new domain. As long as a set of functions is complete, it can be used as a root for an integral transform.

The wavelet transform is a relatively new (integral) transform. What makes this transform special is that the set of basis functions, known as wavelets, are chosen to be well-localized (have compact support) both in space and frequency. Thus, one has some kind of “dual-localization” of the wavelets. This contrasts the situation met for the Fourier Transform where one only has “mono-localization”, meaning that localization in both position and frequency simultaneously is not possible.

The wavelets are parameterized by a *scale parameter* (dilation parameter) $a > 0$, and a *translation parameter* $-\infty < b < \infty$. What makes the wavelet transform remarkable is that the wavelet basis can be constructed from one single function $\psi(x)$ according to

$$\psi_{a;b}(x) = \psi\left(\frac{x-b}{a}\right). \quad (3)$$

In usual terminology, $\psi(x)$ is the mother function or *analyzing wavelet*.

Given a function $h(x)$, the (continuous) wavelet transform is defined as

$$\mathcal{W}[h](a, b) = \frac{1}{\sqrt{a}} \int_{-\infty}^{\infty} \psi_{a;b}^*(x) h(x) dx \quad (4)$$

Here $\psi^*(x)$ denotes the complex conjugate of $\psi(x)$. We should emphasize that some authors use a somewhat different definition when it comes to the prefactor. The specific formulas we derive further on in analyzing the self-affine surfaces depends on the definition we have chosen.

In order for a function $\psi(x)$ to be usable as an analyzing wavelet, one must demand that it has zero mean. However, in nearly all applications it is in addition required to be orthogonal to some lower order polynomials, i.e.,

$$\int_{-\infty}^{\infty} x^m \psi(x) dx = 0, \quad 0 \leq m \leq n. \quad (5)$$

Here the upper limit n is related to what is called the order of the wavelet.

Unlike for instance the more familiar Fourier transform, the wavelet transform is not completely specified before the analyzing wavelet (i.e., the basis) is given. There is a large number of possible candidates, but we will concentrate exclusively on one of the most popular families, namely the Daubechies wavelet family [14].

In order for the wavelet transform to be useful for numerical calculations, it has to be accompanied by an effective numerical implementation. Such an algorithm was developed by Mallat, and the resulting transform is known as the discrete wavelet transform [15].

IV. THE AVERAGED WAVELET COEFFICIENT METHOD

As was shown in Sec. II, the defining feature of self-affine profiles is the scaling property (cf. Eqs. (1) and (2)). According to Eq. (2) one should have $\mathcal{W}[h(x)](a, b) \simeq \mathcal{W}[\lambda^{-H} h(\lambda x)](a, b)$ for a self-affine function $h(x)$ in the wavelet domain. Here, in expressions like $\mathcal{W}[h(x)](a, b)$, we have included the x -dependence explicitly for convenience.

Hence after a simple change of variable one has:

$$\begin{aligned} \mathcal{W}[h(x)](a, b) &\simeq \mathcal{W}[\lambda^{-H} h(\lambda x)](a, b) \\ &= \frac{1}{\sqrt{a}} \int_{-\infty}^{\infty} \lambda^{-H} h(\lambda x) \psi^*\left(\frac{x-b}{a}\right) dx \\ &= \lambda^{-\frac{1}{2}-H} \frac{1}{\sqrt{\lambda a}} \int_{-\infty}^{\infty} h(x') \psi^*\left(\frac{x'-\lambda b}{\lambda a}\right) dx' \\ &= \lambda^{-\frac{1}{2}-H} \mathcal{W}[h(x)](\lambda a, \lambda b). \end{aligned}$$

Thus, we have

$$\mathcal{W}[h](\lambda a, \lambda b) \simeq \lambda^{\frac{1}{2}+H} \mathcal{W}[h](a, b). \quad (6)$$

Note that this scaling relation relies heavily on the definition (4), so for other definitions of the wavelet transform, this equation must be changed accordingly. What the scaling relation (6) expresses, is that if we perform an (isotropic) rescaling (with factor λ) of the wavelet domain of a self-affine function, this is the same as rescaling the wavelet amplitude of the original domain with a factor $\lambda^{\frac{1}{2}+H}$.

From the definition of the wavelet transform, it follows directly that the wavelet domain of a one-dimensional function is two-dimensional; one dimension corresponding to scale and the other to space (translation). So, for instance for a specified scale, we have an infinite number of amplitudes corresponding to various translation parameters b . When one is analyzing self-affine functions, like any fractal, it is the scale rather than the translation which is of

general interest to us. With this in mind, we propose to *average out* the dependency on the translation parameter in the wavelet domain in order to find a representative amplitude at a given scale. We suggest to use the following formula for the average

$$W[h](a) = \langle |\mathcal{W}[h](a, b)| \rangle_b, \quad (7)$$

where $\langle \cdot \rangle_b$ is the standard arithmetic mean value operator with respect to the variable b . Here one could have chosen some other kind of averaging procedure such as geometrical or harmonic means. The absolute value is included in order to get some kind of a “wavelet energy”. The main point is that one gets, by averaging the absolute value of the wavelet coefficients, a representative “wavelet energy” at a given scale. If the dataset is missing data or containing clear anomalies in a region, the average could still be taken over wavelet coefficients corresponding to wavelets localized outside the “damaged” region. However, by doing so we have to drop some of the largest scales completely because they inevitably will include the unwanted region. The Fourier method does not have this nice property, and a missing data region will destroy the whole dataset.

Hence the scaling relation (6) becomes

$$W[h](\lambda a) \simeq \lambda^{\frac{1}{2}+H} W[h](a). \quad (8)$$

The strategy for the data-analysis should now be clear: (1) Wavelet transform the data into the wavelet domain. (2) Calculate the averaged wavelet coefficient $W[h](a)$ according to Eq. (7). (3) Plot $W[h](a)$ against scale a in a log-log plot. A scaling regime consisting of a straight line in this plot implies a self-affine behavior of the data. The slope of this straight line is $\frac{1}{2} + H$.

We call this simple method the *Averaged Wavelet Coefficient* (AWC) method.

V. DATA ANALYSIS WITH THE AVERAGED WAVELET COEFFICIENT (AWC) METHOD

A. Synthetic data

We are now in position to test our scaling relation (8) on artificial and real data, and estimate the corresponding Hurst exponents. We start by performing an AWC-analysis on a set of artificially generated self-affine profiles with predefined Hurst exponents. The self-affine generator used in this work is the Voss algorithm [16], which also is known as the (iterated) midpoint displacement algorithm. The quality of a given analyzing method is assessed by the difference between the Hurst exponent chosen for the Voss-generator, and the estimated value from the analysis.

In our first illustration of the practical performance of the AWC method, we have generated $N = 100$ artificial profiles with Hurst exponent $H = 0.7$ and length $L = 4096$. The wavelet used here and from now on if nothing different is indicated, is the Daubechies wavelet of order 12 (Daub12). We will later demonstrate that this choice of wavelet order, for the Daubechies family¹ For each sample the mean drift of the profile, defined as the line connecting its first and last point, is subtracted. In Fig. 1 the results are presented for both the AWC- and Fourier power spectrum (FPS) density method. In both cases a straight line fit is performed to the (log-log) data, with resulting slopes of respectively 1.19 ± 0.01 and -2.39 ± 0.02 . Theoretically these slopes should be $\frac{1}{2} + H = 1.2$ (cf. Eq. (8)) and $-(1 + 2H) = -2.4$ [12,13] for respectively the AWC- and FPS-method. Hence the corresponding estimated Hurst exponents, in obvious notation, become $H_W = 0.69 \pm 0.01$ and $H_F = 0.70 \pm 0.01$. Here we should emphasize that the errors indicated, are only the regression errors in the actual region. Errors due to different choices of regression regions are not included even if they typically are larger than the regression error itself. The quality of the fit is indicated in Figs. 1a and 1c, by including the fitting function. Empirically we would expect the *total* error of the Fourier power spectral density method to be larger than the corresponding error of the AWC method. This is so because the linear scaling region is smallest for the FPS-method. In order to quantify the behavior for different Hurst exponents, we have performed a corresponding analysis to the above, for various exponents in the range $0 < H < 1$. The results are shown in Figs. 1b and 1d. We observe that there are good agreement between the actual and estimated exponents in the whole range of Hurst exponents independent of method.

¹For wavelets of other types than the Daubechies family, the wavelet order n has to be larger than the Hölder exponent of the strongest singularity present [17,18].

It is often the case that one does not have many data samples available for analysis, especially when dealing with experimental data. To discuss this situation we have performed the same analysis as above, but now with a smaller number of samples; $N = 50$ and $N = 5$ (Fig. 2) and $N = 1$ (Fig. 3). Still the correspondence with the input value is relatively good. However, for small number of samples the uncertainty in the slope determination becomes large, as illustrated in Figs. 3a and 3c. This tendency is much more explicit for the FPS-method than for the AWC-approach.

One could now ask how these results depend on the specific order chosen for actual wavelet. In Fig. 4 we have included a graph showing the AWC-function, $W[h](a)$, for different orders (i.e. smoothness) of the Daubechies wavelet family. With the above comment made on the true error in the Hurst exponent measurements, we conclude that within the actual errors the AWC method does not seem to be sensitive to the order of the wavelet, at least not for the Daubechies wavelet family. A non-systematic study with other kind of wavelets does not change this conclusion.

We have also investigated the situation where the length of the profiles varies. Our findings are compiled in Table I. The results are generally in agreement with the input value for system sizes larger or equal to $L = 256$. It should also be noted that the regression error (not necessarily the actual error) generally decreases with increasing system size. This is as expected because when the system size increases the scaling region becomes larger, resulting in a better regression fit.

In summary, for the study of (clean) synthetic self-affine data, we may conclude that the AWC method works well. It is in particular a good choice when only a few number of samples are available, which is often the case in experimental situations.

B. Stability against noise, drift and distortions

All real measurements are subject to noise, and distortions. These may have their origin in measuring uncertainties, instrumental noise and non-linearities that might transform the signal in some way. The non-linearities may come from the response of the measuring devices used. However, it may also be that the variable studied is not the “good” one. In order for a method of analysis to be useful for real world data, it has to be stable with respect both to noise and distortions.

We start by studying distortions. Suppose that rather than measuring the *generic* self-affine function $h(x)$, we observe $F[h(x)]$, i.e.,

$$h(x) \rightarrow F[h(x)] , \quad (9)$$

which is a one-to-one transformation. This may for example result from distortion of the original signal through the instrumentation. Note that we have not allowed for an explicit x -dependence in F , because this may destroy the self-affinity (more about this later). By other methods it can be demonstrated that the transformation (9) does not change the Hurst exponent [4]. A qualitative way to understand this result is that, since the Hurst exponent H is related to the tendency of dh to change sign (see earlier discussion), the Hurst exponent should be insensitive to transformations of the type (9) as long as F is a relatively smooth functional. To demonstrate the stability of the AWC method to such distortions, we have performed a numerical experiment, where we have put $F[h(x)] = \log_{10}(h(x))$, and then calculated the Hurst exponent from $F[h(x)]$. The result is shown in Fig. 5, and as can be seen, the Hurst exponent is unchanged within the numerical errors. The logarithmic function is a highly non-linear function, something which thus changes the input data dramatically, thus providing a good testing ground of this assumption.

In many situations one has signals possessing some kind of drift. It has earlier been shown that such drifts can dramatically influence the reliability of the measured Hurst exponent [19]. In order to test our method in this respect, we have performed an analysis where we have added linear (Figs. 6a and b) and quadratic drift (Figs. 6c and d) to the self-affine component of the data. In this part of the analysis we have not subtracted the line connecting the first and last point of our dataset ahead of the wavelet transform as described earlier. For the linear case, there is only a weak dependence, independent of scale, on the drift of the data (Figs. 6a and b). However, for the quadratic case, the situation is somewhat different. Here the drift creates a nice crossover between the self-affine region, dominating at small scales, and the drift at large scales. This can be easily seen from Fig. 6d. The Hurst exponent obtained from the small-scale region is $H = 0.71 \pm 0.05$, which fits quite well to the exponent, $H = 0.70$, of the self-affine component of the data. In both cases the amplitude of the drift seems to be of secondary importance. Based on the above, we conclude that our method seems to work quite well for data with drift.

It is easy to see that if the functional F has some explicit dependence on the “horizontal” coordinate (i.e. x in our case), the self-affine correlation property may be destroyed. Spatial noise of any kind, has exactly this property. Since such noise is usually always found in real data, it is important to investigate how sensitive the AWC-algorithm

is to such artefacts. In order to simulate this situation, we apply the functional $F[h(x), x] = h(x) + \eta(x)$, where $\eta(x)$ is a noise term, to clean self-affine data $h(x)$, and then proceed with the AWC analysis. The amount of noise added to the data, i.e., the noise rate χ , is defined as $\chi = (\max|\eta(x)| - \min|\eta(x)|)/(\max|h(x)| - \min|h(x)|)$.

In this paper we have chosen to work with white, pink ($1/f$) and brown ($1/f^2$) noise. Quite recently Aguilar and coworkers have pointed out that scanning tunneling microscopy instrument noise is pink [20]. The quantitative effect of adding $\chi = 10\%$ noise to a given self-affine profile is demonstrated in Fig. 7. The results of the AWC-analysis for the case $\chi = 10\%$ of added white, pink or brown noise are shown in respectively Fig. 8, Fig. 9 and Fig. 10. In all cases (with $\chi = 10\%$) we see that the AWC method extracts the actual Hurst exponent quite well. Notice that for the white noise case, only the lower scales seem to be considerably affected, if any, by the noise. It should be observed that for $H = 0.7$ (see Fig. 8a) a nice crossover to the (now smaller) scaling regime is shown, while for $H = 0.2$ (Fig. 8b) this crossover is not visible. This behaviour we have found to be quite systematic in the sense that the higher Hurst exponents (in the range $0 < H < 1$) the more pronounced was the crossover, and the smaller was the (self-affine) scaling regime. The explanation for this behaviour is the following: For Hurst exponents in the lower range $0 < H < 0.5$, (i.e. anti-correlation) the profiles are quite spiky with sharp tops and deep valleys. This means that the wavelet coefficients at low scales become large for low Hurst exponents with the consequence that the contribution of the noise is suppressed. As the Hurst exponent gets larger, and thus the profiles become more smooth, the effect of the noise at small scales will becomes more and more important resulting in a well-defined crossover. This crossover is easily seen in Fig. 8a.

For the white noise case, we just saw that mainly the small scales were affected, if any, by the noise. This situation is somewhat different for the pink and brown noise cases (see Figs. 9 and 10). For these two noise types the whole region is affected without, for $\chi = 10\%$, introducing significant changes over the non-noisy results (Figs. 9–10b). As the noise level increases (see Figs. 9–10d) larger deviation from the none-noisy case starts to emerge. By noting that pink and brown noise is nothing but self-affine signals with Hurst exponents of respectively $H = 0$ and $H = 0.5$, we would expect that the estimated exponents are shifted towards these values. This is supported by the observation from Figs. 9d and 10d that the slopes, for a noisy $H = 0.7$ profiles seems to decrease with increasing noise level χ . It should also be observed that there seems to be a more well-developed crossover for the pink than the brown case. This stems from the fact that Figs. 9d and 10d are shown for $H = 0.7$, giving the better “contrast” for the pink limiting case of $H = 0$.

Self-affine scaling behavior is usually only found over a limited region of space (or time), and it is important to be able to estimate these crossover scales. To be able to investigate the potential of the AWC method in this respect, we have generated some artificial self-affine profiles with $H = 0.7$ and length $L = 4096$ and used a standard 5-point filter to destroy the self-affine correlations at small distances (i.e. destroy correlations between 11 subsequent points). For the AWC method we should expect to see a crossover at scales $a_c = \simeq 0.003$, while for the FPS-method the crossover frequency is expected at $f_c = 0.09$. As can be seen from Fig. 11, this is indeed what we find. For the largest number of sample ($N = 100$) the AWC and FPS method are equivalent, but for only one sample the crossover is most easily seen for the wavelet method as shown in Figs. 11c and d.

C. Real data

As mentioned in the introduction, self-affine surfaces can be found many places in the sciences. Here we will in particular discuss two quite different examples, clearly demonstrating the general presence of self-affine structures.

Our first example is taken from geology, and concerns the structure of a fractured granite surface [21]. The surface contains 2050×211 data points. One representative profile of this surface is given in Fig. 12a. The results of the wavelet and Fourier analysis, using the methods described earlier in this paper, are collected in Figs. 12b and c. We see that there are nice scaling regions in both cases indicating that the fractured granite surface is indeed self-affine. The Hurst exponents, obtained by a regression fit to the scaling region, are $H_W = 0.81 \pm 0.02$ and $H_F = 0.79 \pm 0.03$ respectively for the AWC and FPS method. Note that also here only the regression error is indicated and that the “true error” is somewhat larger. The results for the two methods are consistent and coincide with the results of other studies of fracture granite surfaces [22]. The reason for the good agreement between the two methods, and the good quality of both regression fits are due mainly to the large number of samples available, as the dataset contains 211 one-dimensional profiles of length 2050. It is interesting to observe that the exponent for the fractured granite surface reported here, is in complete agreement with earlier speculations that fracture surfaces should have a universal Hurst exponent of $H = 0.8$ [3,23,24].

Unfortunately, the availability of large number of samples is rare. nor is it appropriate to talk about several samples at all in some situations. In order to illustrate this point, we have included share prices for the Italian automobile

manufacturer FIAT taken from the Milan Stock Exchange for the period from the 1st of September 1988 to the 28th of May 1991 with three quotes per day [25] (Fig. 13a). Observe that here only one sample for a given time period is available. The result of the corresponding analysis is given in Figs. 13b and c. The estimated Hurst exponents are $H_W = 0.65 \pm 0.03$ and $H_F = 0.62 \pm 0.06$ from respectively the AWC and FPS method. These two results are consistent, but there are noticeable difference in the accuracy of the regression fits for the two methods. This is most easily seen by comparing Figs. 13b and c by visual inspection. The error bars associated with the FPS analysis, based solely on the regression analysis, are in particular underestimated. It is difficult to identify a scaling region at all. We find it very interesting to observe that a Hurst exponent $H = 0.65$ is observed in the stock market simulations by Bak et al. [6] when using the Urn model with volatility feedback.

This example, is in our view, a very good example of the power of the AWC method in cases where few samples are available, and we believe it to have potential of becoming a useful method in practical situations.

VI. CONCLUSIONS

We have introduced, derived and tested a new simple method for Hurst exponent measurements based on the wavelet transform. It has been compared to the Fourier power spectrum method where appropriate. We find that the two methods performs approximately equally for large number of samples. However, for small numbers of samples this new method outperforms the more traditional Fourier transform based method. The AWC method are also demonstrated to handle noisy and experimental data in a satisfactory manner.

ACKNOWLEDGMENTS

We are grateful to J. Schmittbuhl for permission to use his measurements for the fractured granite surface. We also thank B. Vidakovic for providing us with the Fiat share price data. One of the authors (I. S.) thanks the Research Council of Norway and Norsk Hydro AS for financial support. This work has received support from the Research Council of Norway (Program for Supercomputing) through a grant of computing time.

- [1] P. Meakin, Phys. Rep. **235**, 189 (1993).
- [2] L. Barabasi and H. E. Stanley, *Fractal Growth Models* (Cambridge University Press, Cambridge, 1995).
- [3] E. Bouchaud, G. Lapasset and J. Planès, Europhys. Lett, **13**, 73 (1990).
- [4] A. Hansen and O. M. Nes, *IKU Report*, unpublished, 1997.
- [5] T. Vicsek, M. Cserzö and V. K. Horváth, Physica A **167**, 315 (1990).
- [6] P. Bak, M. Paczuski and M. Shubik, cond-mat/9609144, 1996.
- [7] J. Schmittbuhl, J. P. Villette, and S. Roux, Phys. Rev. E **51**, 131 (1995).
- [8] A. Arneodo, E. Bacry and J. F. Muzy, Physica A **213**, 232 (1995).
- [9] C. J. Jones, G. T. Lonergan and D. E. Mainwaring, J. Phys. A **29**, 2509 (1996).
- [10] Z.R. Struzik, Fractals **3**, 329 (1995).
- [11] Z.R. Struzik, Fractals **4**, 469 (1996).
- [12] J. Feder, *Fractals* (Plenum, New York, 1988).
- [13] K. Falconer, *Fractal geometry: mathematical foundations and applications* (John Wiley, Chichester, 1990).
- [14] I. Daubechies, *Ten Lectures on Wavelets* (SIAM, Philadelphia, 1992).
- [15] W. H. Press, S. A. Teukolsky, W. T. Vetterling and B. P. Flannery, *Numerical Recipes*, 2nd edition (Cambridge University Press, Cambridge, 1992).
- [16] R.F. Voss, *Scaling phenomena in disordered Systems* (Plenum, New York, 1985).
- [17] S. Mallat and W.L. Hwang, IEEE Trans. on Inform. Theory **38**, 617 (1992).
- [18] J.F. Muzy, E. Bacry and A. Arneodo, Int. J. of Bifurcation and Chaos, **4**, 215 (1994).
- [19] A. Hansen, T. Engøy and K.J. Måløy, Fractals **2**, 527 (1994).
- [20] M. Aguilar, E. Anguiano, F. Vazquez and M. Pancorbo, J. Microscopy **167**, 197 (1992).
- [21] J. Schmittbuhl, unpublished (1997).
- [22] J. Schmittbuhl, S. Roux and Y. Berthaud, Europhys. Lett. **28**, 585 (1994).
- [23] K. J. Måløy, A. Hansen, E. L. Hinrichsen and S. Roux, Phys. Rev. Lett. **68**, 213 (1992).

- [24] E. Bouchaud, G. Lapasset, J. Planès and S. Navéos, Phys. Rev. B **48**, 2917 (1993).
[25] Data from B. Vidakovic, <http://www.isds.duke.edu/~brani/datapro.html>.

<i>L</i>	<i>H</i> _F	<i>H</i> _W
64	0.57 ± 0.04	0.67 ± 0.05
128	0.65 ± 0.03	0.66 ± 0.03
256	0.66 ± 0.01	0.69 ± 0.02
512	0.66 ± 0.02	0.70 ± 0.02
1024	0.70 ± 0.01	0.70 ± 0.01
2048	0.70 ± 0.01	0.70 ± 0.01
4096	0.70 ± 0.01	0.70 ± 0.01

TABLE I. Estimated Hurst exponents for the FPS- (*H*_F) and AWC-method (*H*_W) for different system sizes, *L*. The predefined Hurst exponent was *H* = 0.7, and in all calculations the number of samples used was *N* = 100. The wavelet used was Daub12.

FIG. 1. Hurst exponents estimated by (a and b) the averaged wavelet method (*H*_W) and (c and d) the Fourier power spectrum density method (*H*_F). All errorbar in this, and later figures, are regression errors only. (a) The AWC-function *W*[*h*](*a*) vs scale *a* for Hurst exponent *H* = 0.7. The solid line is the regression line to the scaling region. The estimated Hurst exponent is *H*_W = 0.69 ± 0.01. (b) Wavelet estimated Hurst exponents (*H*_W) for various actual Hurst exponents *H*. (c) The power spectrum, *P*(*f*) vs frequency *f* for actual Hurst exponent *H* = 0.7. The solid line is the regression fit. The estimated Hurst exponent is *H*_F = 0.70 ± 0.01. (d) Fourier estimated Hurst exponents (*H*_F) for various actual Hurst exponents *H*. The number of samples per data point was *N* = 100, and the length of the profiles were *L* = 4096. The same profiles were used for both the wavelet and Fourier analysis.

FIG. 2. The same as Fig. 1b and d, but now with the following number of samples *N* = 50 (a and b) and *N* = 5 (c and d).

FIG. 3. The same as Fig. 1, but now with only one sample, *N* = 1.

FIG. 4. The AWC-function *W*[*h*](*a*) vs scale *a*, for various choices of wavelet order (Daubechies family) as indicated in the figure. The data are for self-affine profiles with Hurst exponent *H* = 0.7, and the number of samples used was *N* = 100. The length of the profiles was *L* = 4096. The extracted Hurst exponents were *H* = 0.68 ± 0.01 for daub4, and *H* = 0.70 ± 0.01 in all other cases.

FIG. 5. (a) The AWC-function *W*[*g*](*a*) vs scale *a* where *g*(*x*) = *log*₁₀(*h*(*x*)) and *h*(*x*) is a self-affine function with *H* = 0.7. The number of samples used was *N* = 100, and length of the profiles was *L* = 4096. The solid line is the regression fit to the data, and the estimated Hurst exponent was *H*_W = 0.70 ± 0.01 (b) Wavelet measured Hurst exponents, *H*_W, for various actual exponents in the range 0.1 ≤ *H* ≤ 0.9.

FIG. 6. The Figures show the effect of added linear (a and b) and quadratic (c and d) drift to the data. In all cases the self-affine component of the data had *H* = 0.7. (a) One sample with linear drift (*y*(*x*) = 0.5*x*). (b) The AWC-function *W*[*h*](*a*) vs scale *a* for data with linear drift of the type showed in Fig. a. The number of samples used was *N* = 100 and the length of the all profiles was *L* = 4096. The full line is the regression line. The extracted Hurst exponent is *H* = 0.70 ± 0.01. (c and d) The same as Figs. (a) and (b) respectively, but now for quadratic drift (*y*(*x*) = 0.05*x*²). In Fig. (c) we have also included the drift separately (the dashed line). Notice the well-developed crossover between the larger and smaller scales in Fig. (d). The extracted Hurst exponent is *H* = 0.71 ± 0.05. The slope, *α* of the regression line (dot-dashed) for the large scales is *α* = 2.29 ± 0.04.

FIG. 7. (a) shows a self-affine profile with *H* = 0.7. To this profile we add χ = 10% white (b), pink (c), and brown (d) noise. The lower curve in Figs. (b)–(d) is the added noise.

FIG. 8. The Figures show the effect of white noise added to the self-affine component of the data. The AWC-function $W[h](a)$ vs scale a for the self-affine component of the data with $H = 0.7$ and $H = 0.2$ and a noise level $\chi = 10\%$ (a and b). The estimated Hurst exponents for the curves shown in Figs. (a) and (b) were respectively $H_W = 0.71 \pm 0.02$ and $H_W = 0.21 \pm 0.01$. The extracted Hurst exponents with regression errors for Hurst exponents in the range $0 < H < 1$ and step 0.1 (c). The effect of the noise on the AWC-function, $W[h](a)$, for various noise levels χ as indicated in the figure (d). The Hurst exponent of the self-affine component was $H = 0.7$ in this case. The number of samples per data point was $N = 100$, and the length of the profiles was $L = 4096$.

FIG. 9. The same as Fig. 8, but now pink noise added. The estimated Hurst exponents for the curves shown in Figs. (a) and (b) are respectively $H_W = 0.69 \pm 0.01$ and $H_W = 0.21 \pm 0.01$.

FIG. 10. The same as Fig. 8, but now brown noise added. The estimated Hurst exponents for the curves shown in Figs. (a) and (b) are respectively $H_W = 0.69 \pm 0.01$ and $H_W = 0.19 \pm 0.01$.

FIG. 11. The wavelet (Figs. (a) and (c)) and Fourier (Figs. (b) and (d)) analysis of synthetic data with Hurst exponent $H = 0.7$ after applying a 5-point filter to them. In Figs. (a) and (b), the results are averaged over $N = 100$ samples, while in Figs. (c) and (d) only one sample ($N = 1$) is used. In all cases $L = 4096$. The solid lines are the regression fits to the scaling regions. The crossovers are clearly seen in all cases. Theoretically the crossover values are $a_c = 0.003$ and $f_c = 0.09$ for the wavelet and Fourier method respectively.

FIG. 12. (a) One single representative profile from the granite fracture. The number of points in the profile is $L = 2050$. (b) AWC analysis of the entire set of (2050×211) data points. The solid line is the regression fit to the scaling region. The corresponding Hurst exponent is $H_W = 0.81 \pm 0.02$. (c) FPS analysis of the data. Here the solid line corresponds to a Hurst exponent $H_F = 0.79 \pm 0.03$.

FIG. 13. (a) Fiat share prices taken from the Milan Stock Exchange for the period from the 1st of September 1988 (day 1) to the 28th of May 1991, with three observation per day. (b) The result of the wavelet analysis for the data in (a). The estimated Hurst exponent, corresponding to the solid line, is $H_W = 0.65 \pm 0.03$. (c) The result of the Fourier analysis for the data in (a). The Hurst exponent in this case is $H_F = 0.62 \pm 0.06$. Note the more well-behaved scaling region for the wavelet method as compared to the Fourier method.

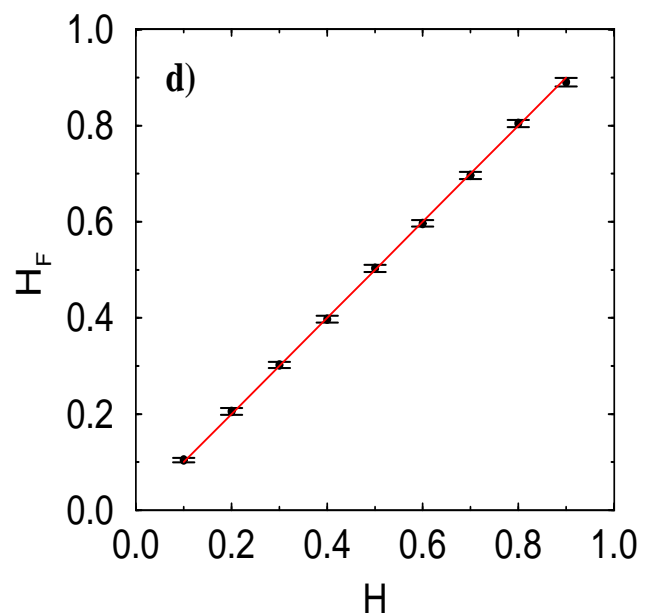
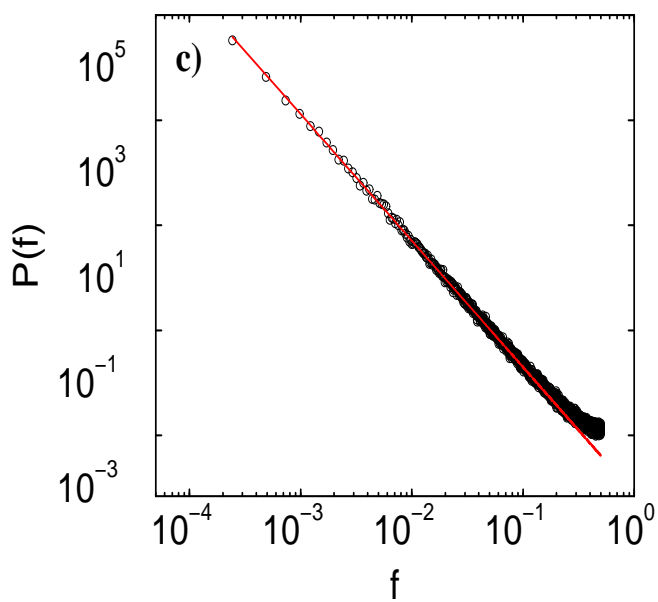
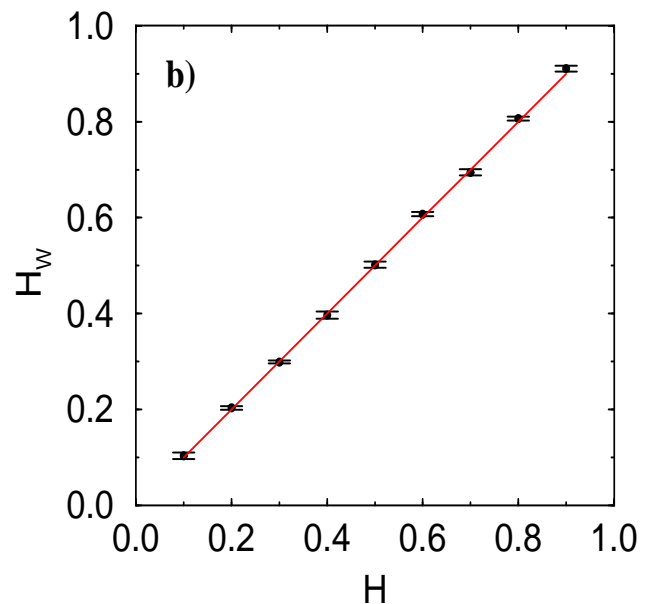
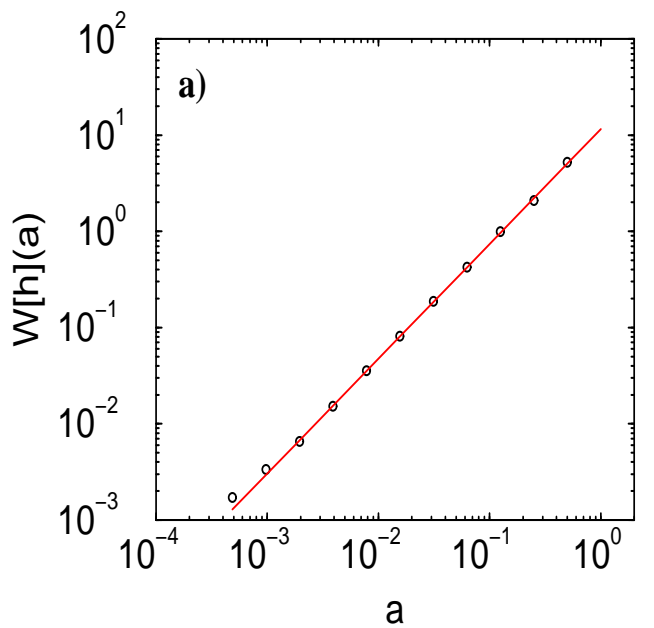


Figure 1
 Simonsen, Hansen and Nes
Determination of the Hurst Exponent by use of Wavelet Transforms

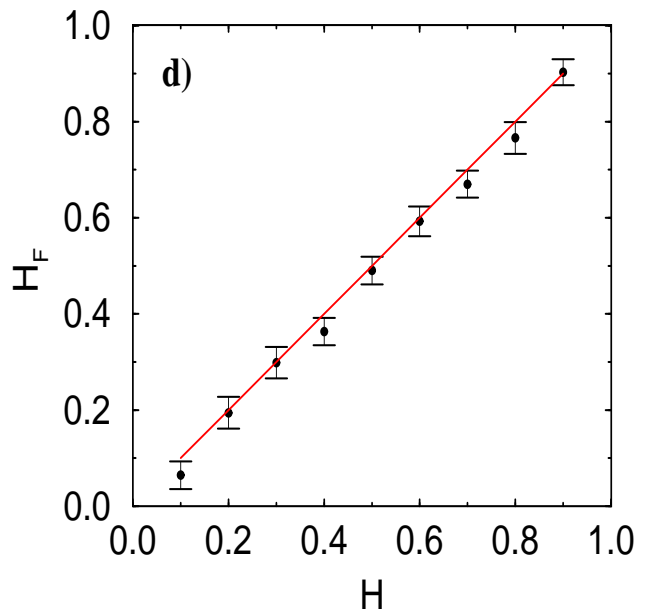
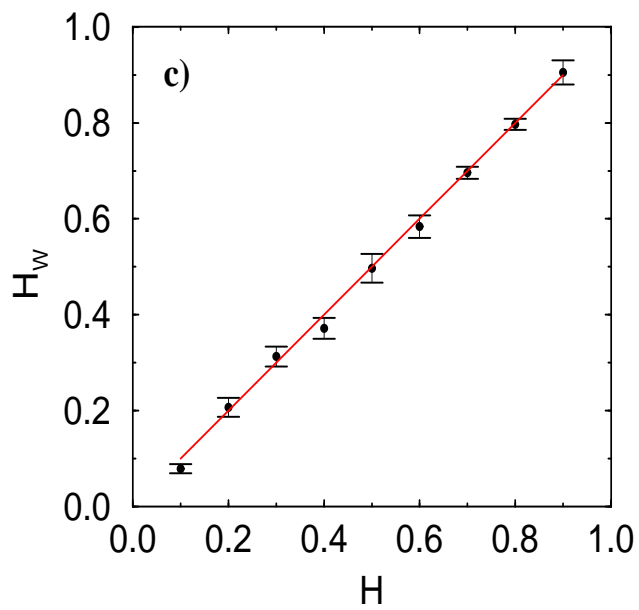
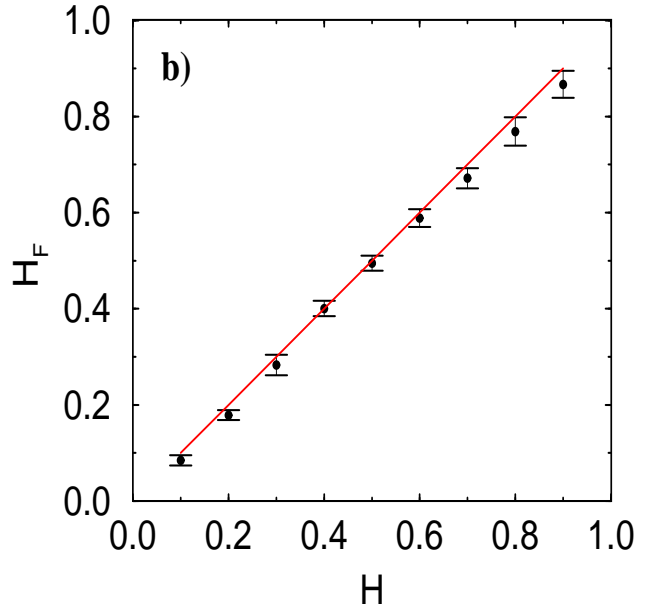
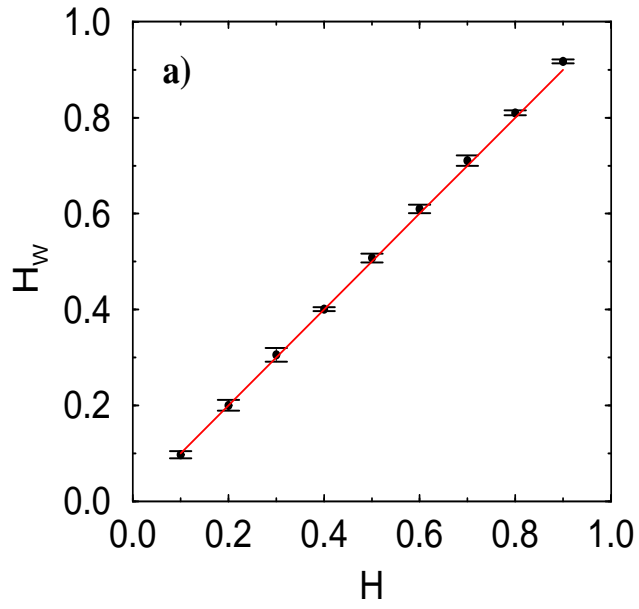


Figure 2
Simonsen, Hansen and Nes
Determination of the Hurst Exponent by use of Wavelet Transforms

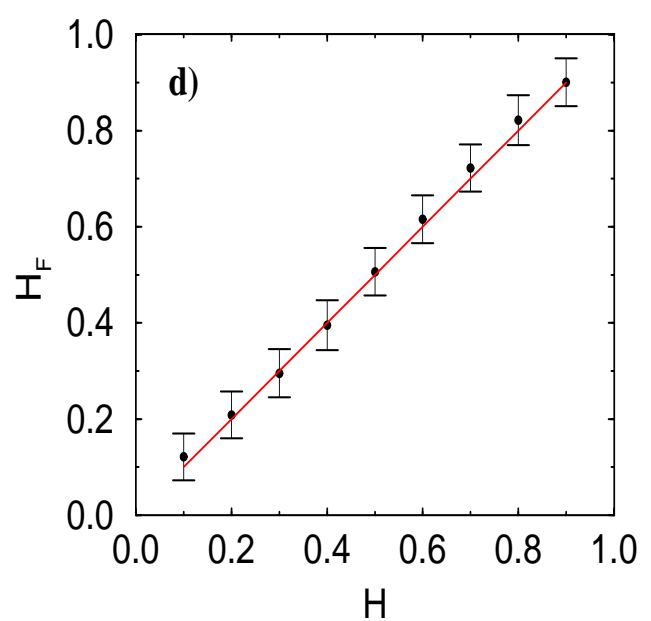
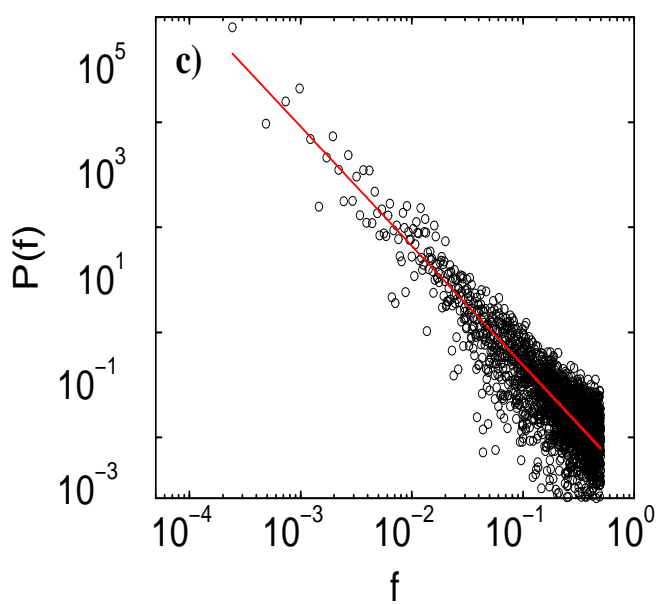
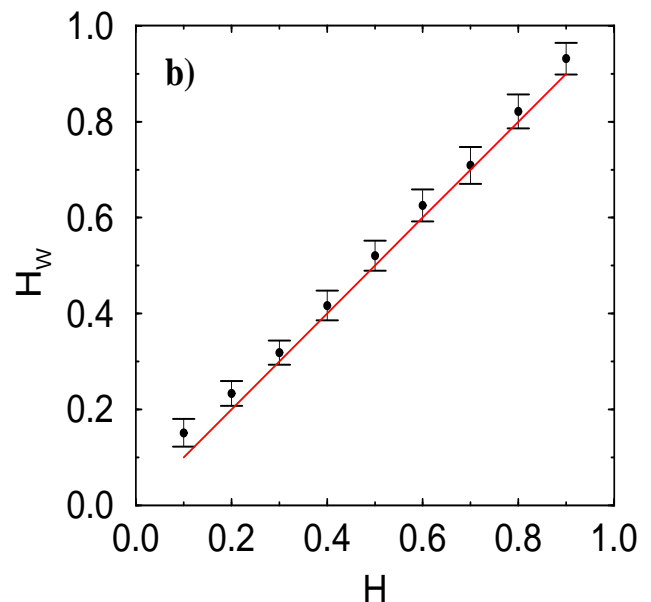
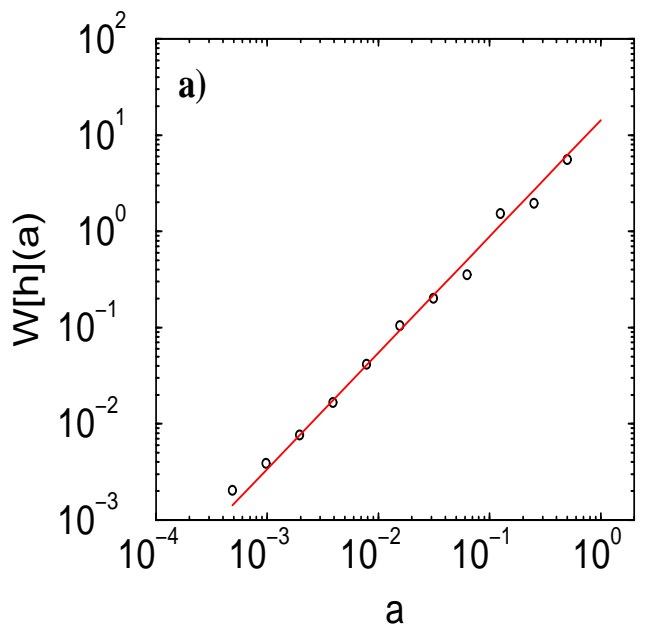


Figure 3
 Simonsen, Hansen and Nes
Determination of the Hurst Exponent by use of Wavelet Transforms

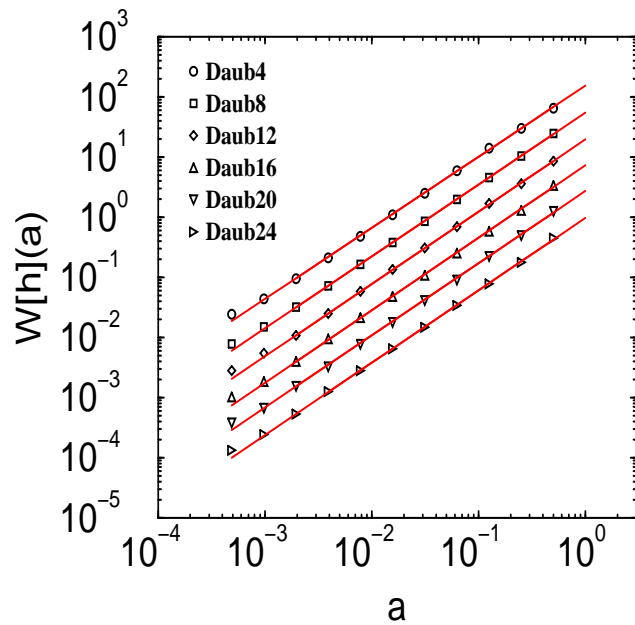


Figure 4
 Simonsen, Hansen and Nes
Determination of the Hurst Exponent by use of Wavelet Transforms

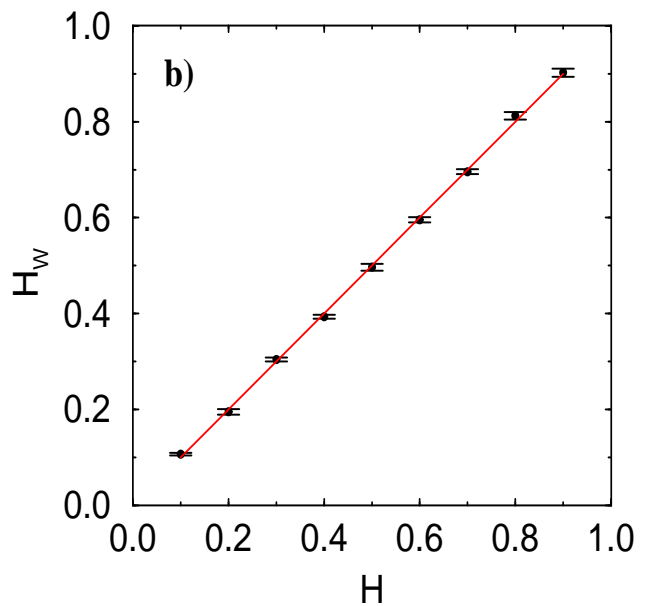
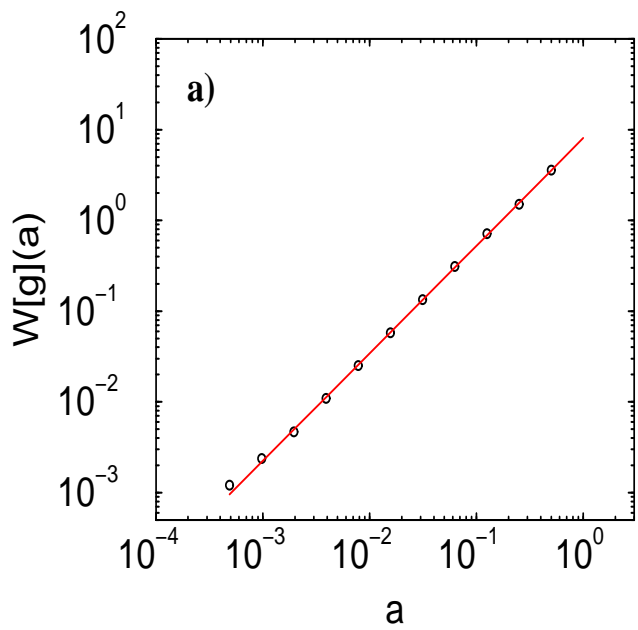


Figure 5
Simonsen, Hansen and Nes
Determination of the Hurst Exponent by use of Wavelet Transforms

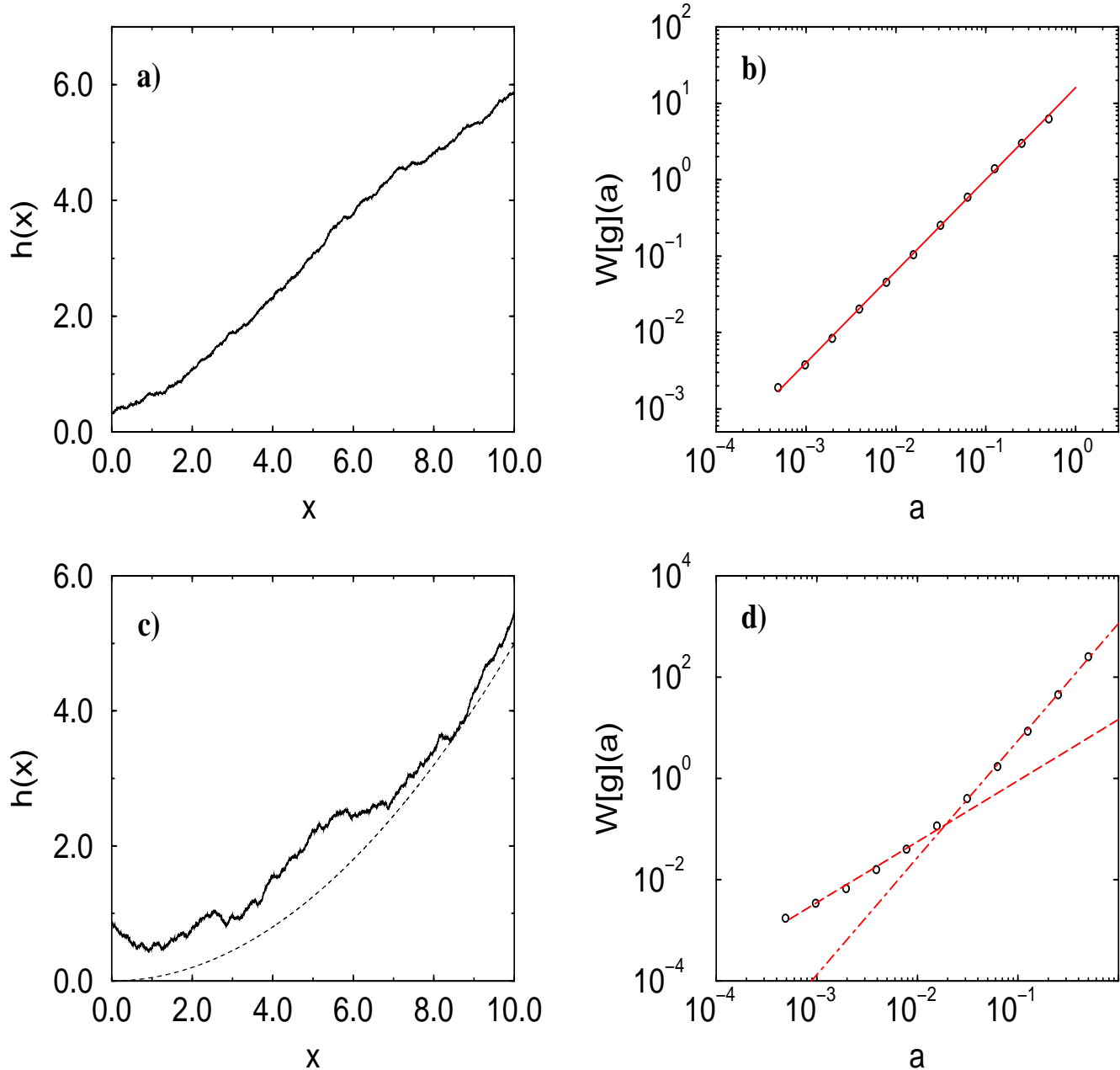


Figure 6
 Simonsen, Hansen and Nes
Determination of the Hurst Exponent by use of Wavelet Transforms

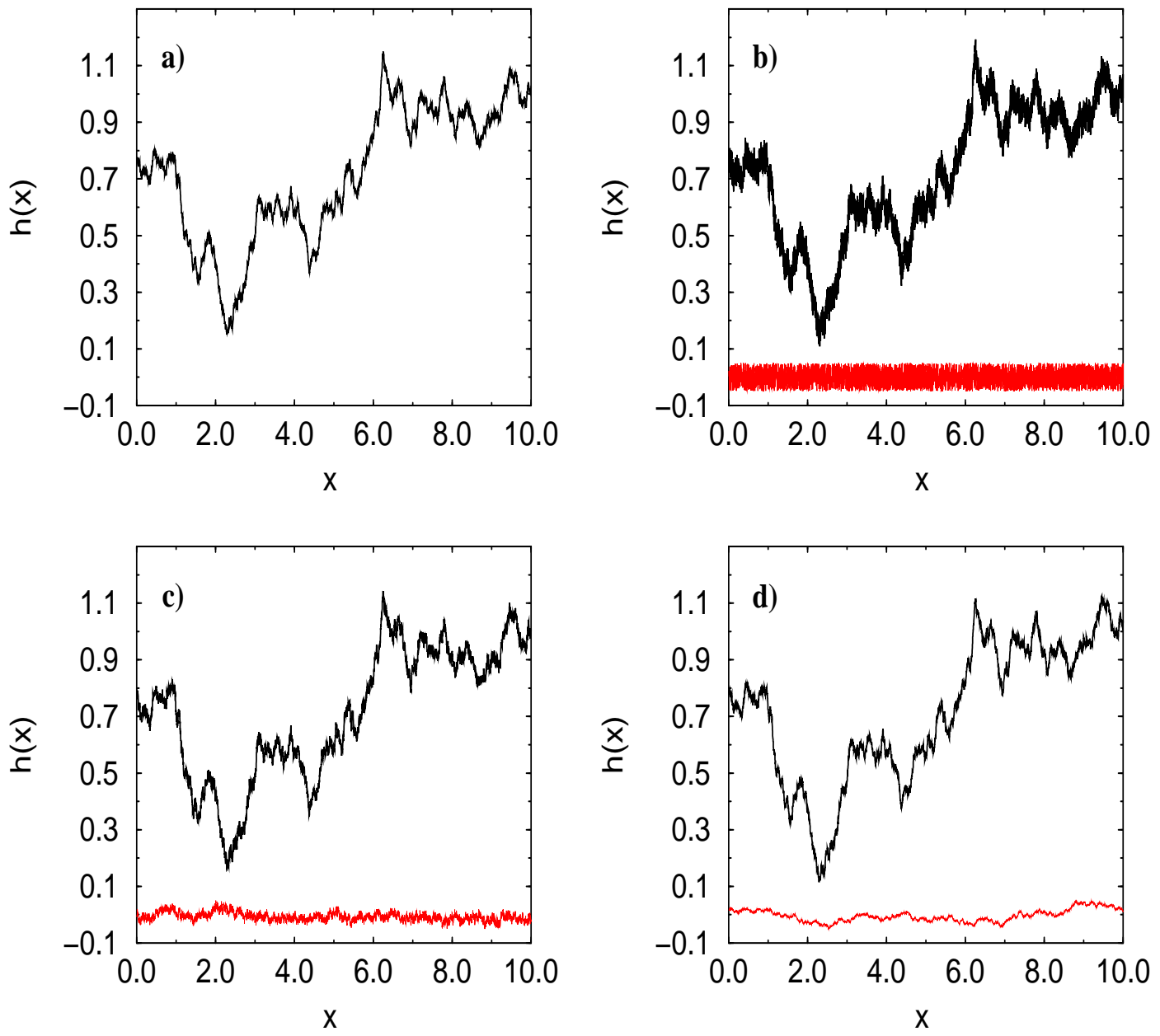


Figure 7
 Simonsen, Hansen and Nes
Determination of the Hurst Exponent by use of Wavelet Transforms

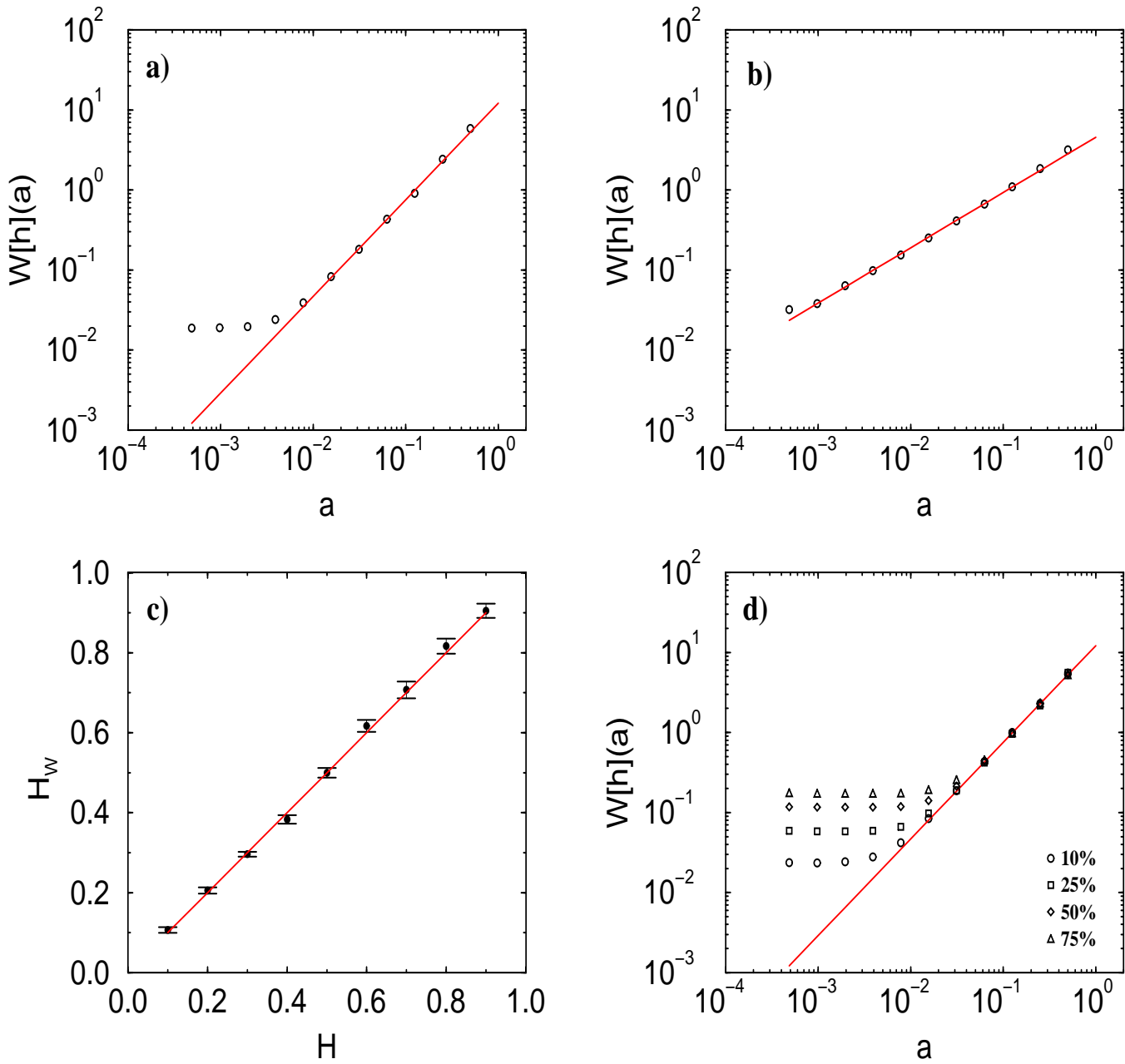


Figure 8
 Simonsen, Hansen and Nes
Determination of the Hurst Exponent by use of Wavelet Transforms

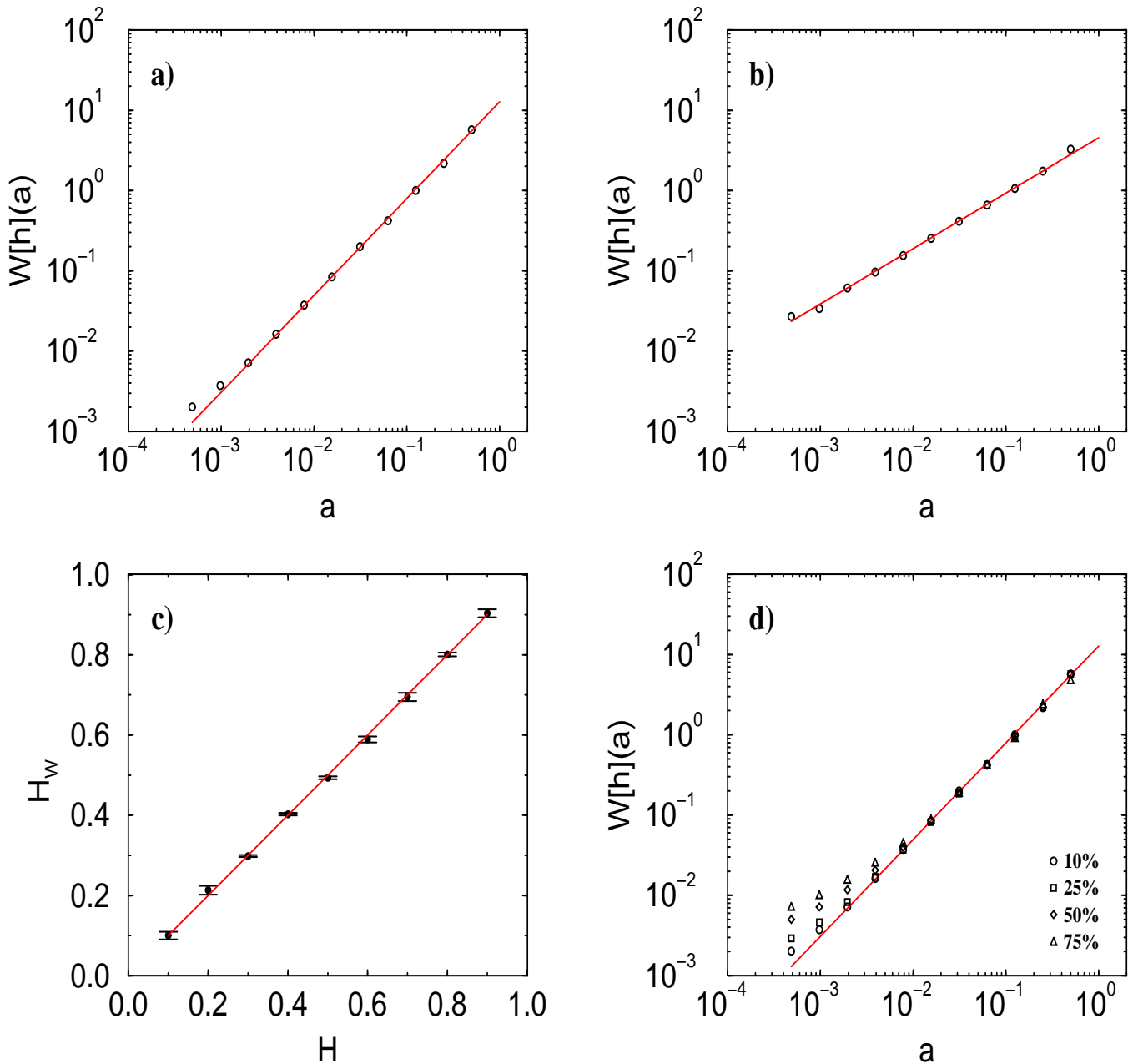


Figure 9
 Simonsen, Hansen and Nes
Determination of the Hurst Exponent by use of Wavelet Transforms

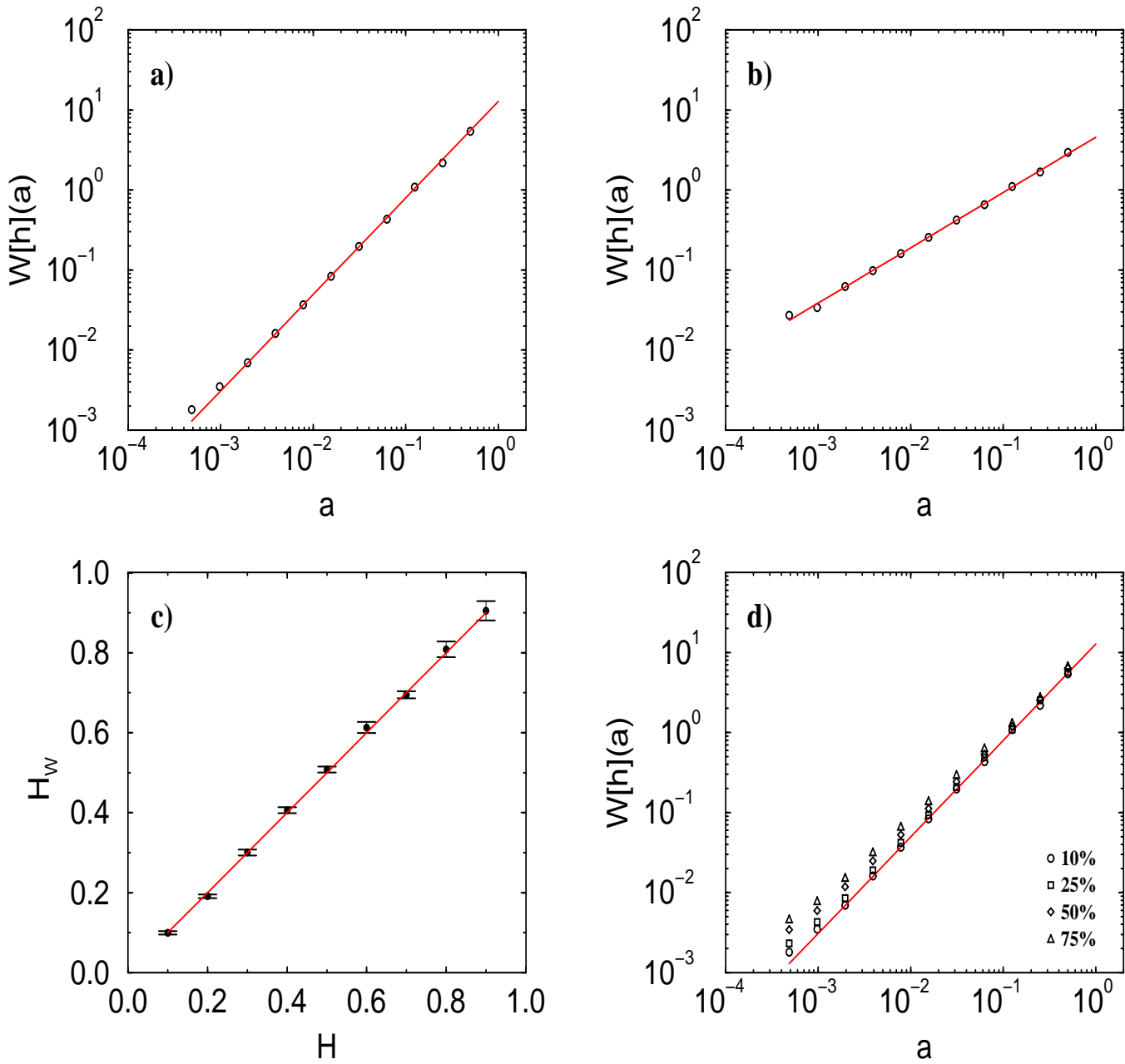


Figure 10
 Simonsen, Hansen and Nes
Determination of the Hurst Exponent by use of Wavelet Transforms

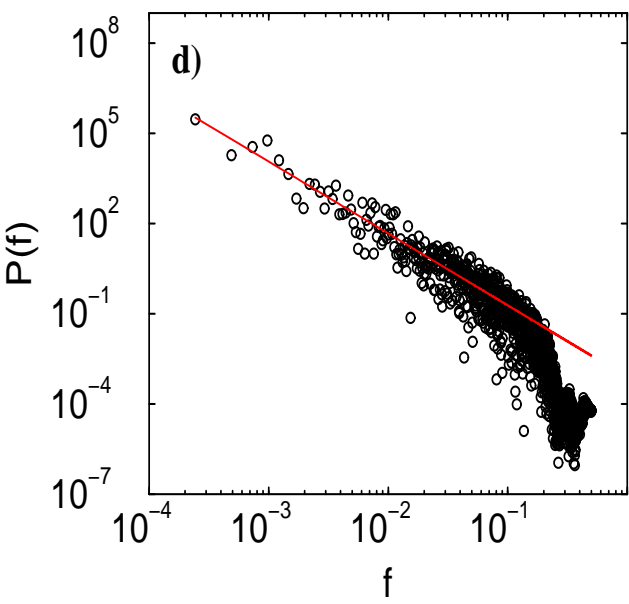
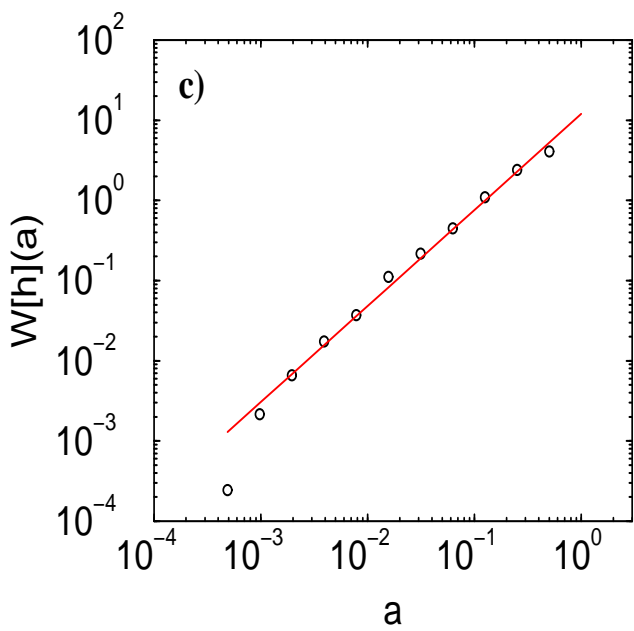
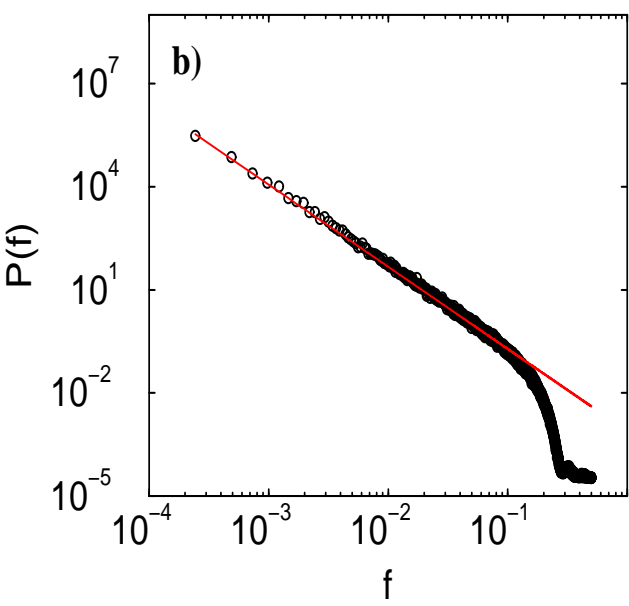
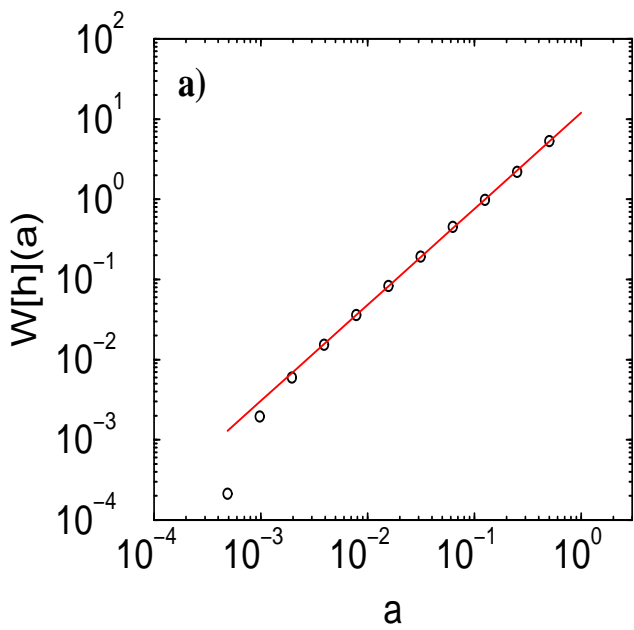


Figure 11
 Simonsen, Hansen and Nes
Determination of the Hurst Exponent by use of Wavelet Transforms

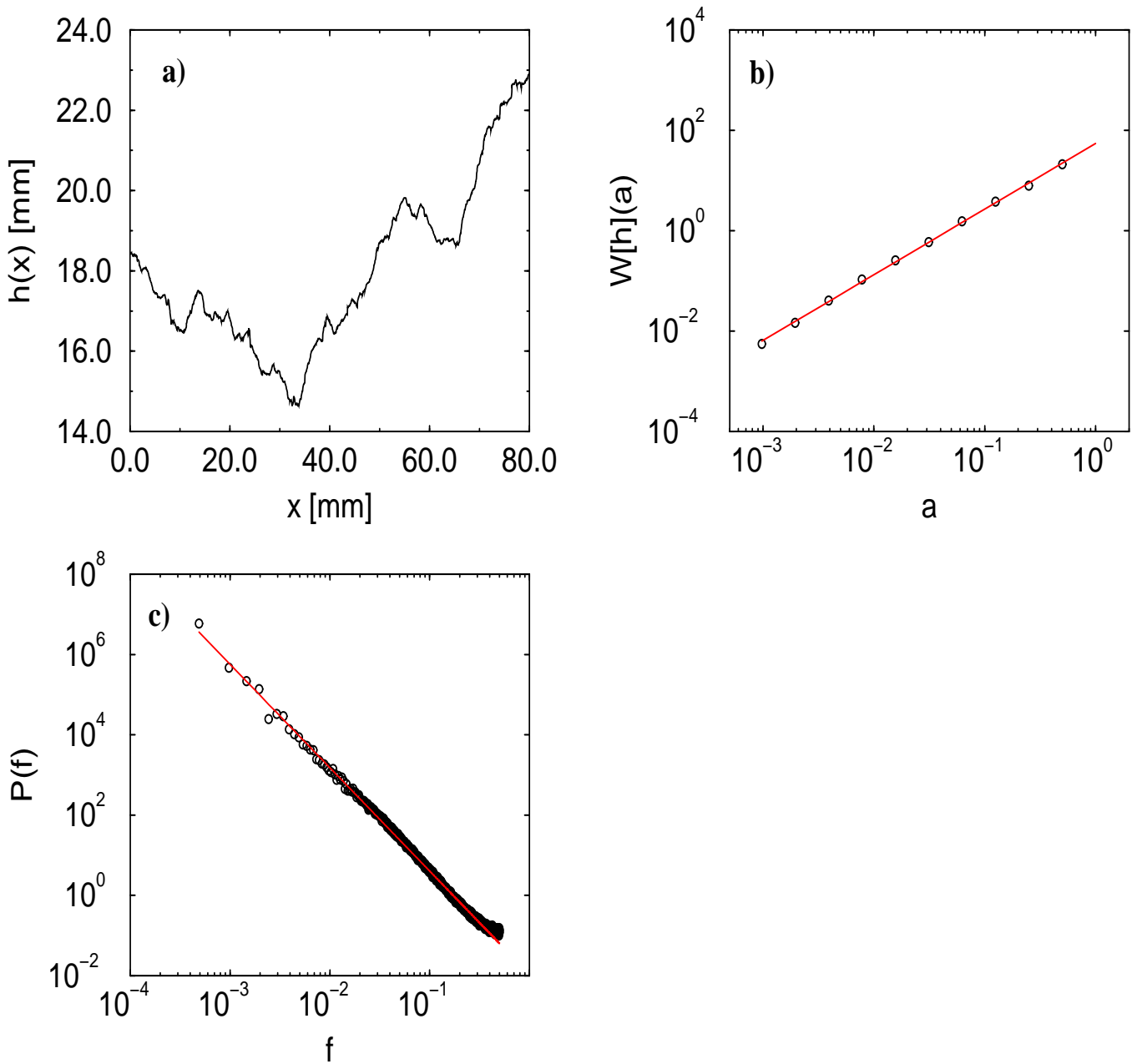


Figure 12
 Simonsen, Hansen and Nes
Determination of the Hurst Exponent by use of Wavelet Transforms

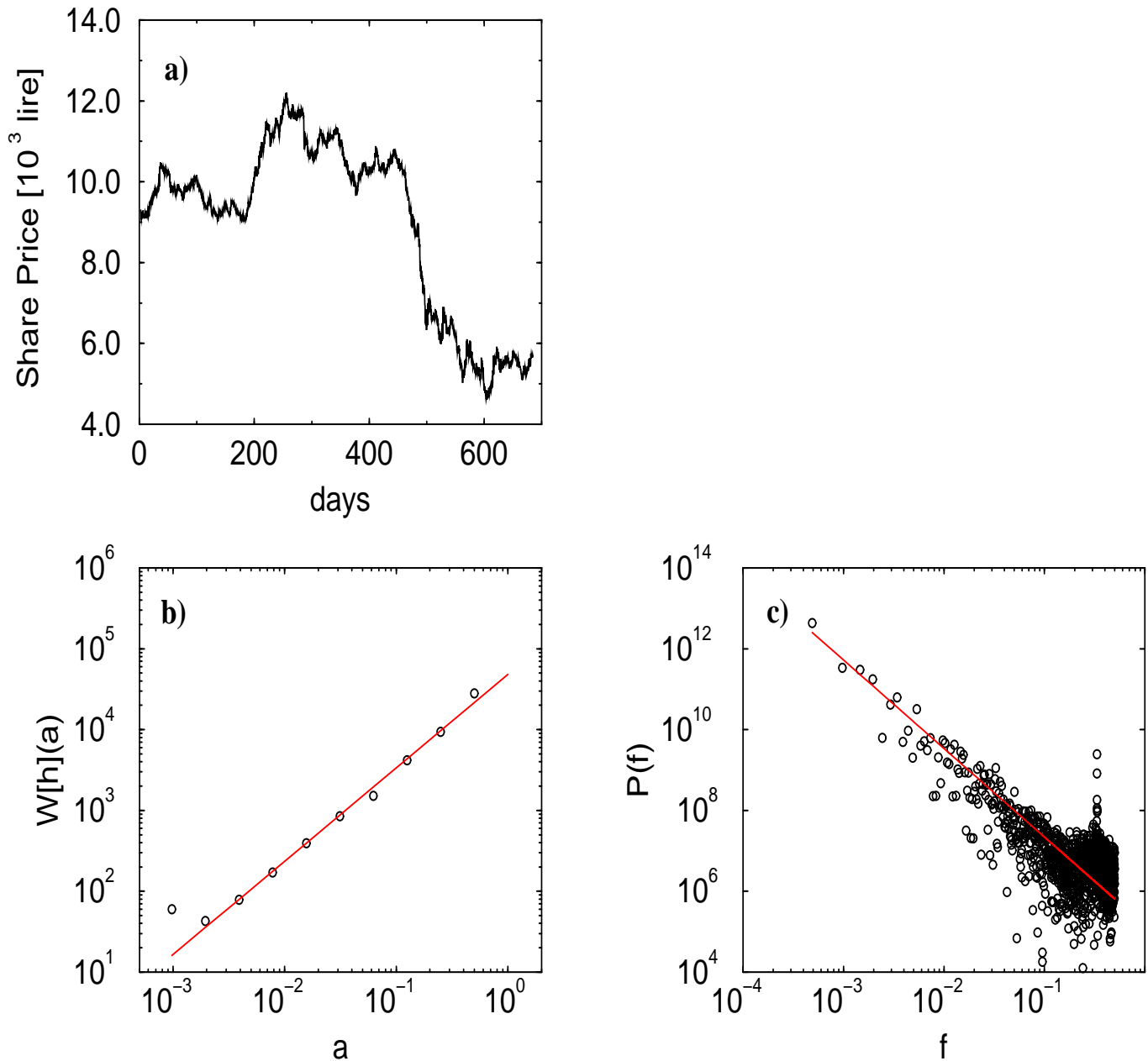


Figure 13
 Simonsen, Hansen and Nes
Determination of the Hurst Exponent by use of Wavelet Transforms